J Mater Sci (2020) 55:203–217

Computation & theory

Ab initio calculations of $CaZrO_3$ (011) surfaces: systematic trends in polar (011) surface calculations of ABO_3 perovskites

Roberts I. Eglitis[1,*], J. Kleperis[1], J. Purans[1], A. I. Popov[1], and Ran Jia[1,2]

[1] Institute of Solid State Physics, University of Latvia, 8 Kengaraga Str., Riga 1063, Latvia
[2] Laboratory of Theoretical and Computational Chemistry, Institute of Theoretical Chemistry, Jilin University, Changchun 130023, People's Republic of China

Received: 7 May 2019
Accepted: 10 September 2019
Published online: 23 September 2019

ABSTRACT

By means of the CRYSTAL computer program package, first-principles calculations of polar ZrO-, Ca- and O-terminated $CaZrO_3$ (011) surfaces were performed. Our calculation results for polar $CaZrO_3$ (011) surfaces are compared with the previous ab initio calculation results for ABO_3 perovskite (011) and (001) surfaces. From the results of our hybrid B3LYP calculations, all upper-layer atoms on the ZrO-, Ca- and O-terminated $CaZrO_3$ (011) surfaces relax inwards. The only exception from this systematic trend is outward relaxation of the oxygen atom on the ZrO-terminated $CaZrO_3$ (011) surface. Different ZrO, Ca and O terminations of the $CaZrO_3$ (011) surface lead to a quite different surface energies of 3.46, 1.49, and 2.08 eV. Our calculations predict a considerable increase in the Zr–O chemical bond covalency near the $CaZrO_3$ (011) surface, both in the directions perpendicular to the surface (0.240*e*) as well as in the plane (0.138*e*), as compared to the $CaZrO_3$ (001) surface (0.102*e*) and to the bulk (0.086*e*). Such increase in the B–O chemical bond population from the bulk towards the (001) and especially (011) surfaces is a systematic trend in all our eight calculated ABO_3 perovskites.

Introduction

Surface and interface phenomena, taking place in the ABO_3 perovskites and their nanostructures, as well as mechanisms of various (001) and (011) surface electronic processes, are the key topics in theoretical solid-state physics [1–27]. $CaTiO_3$, $SrTiO_3$, $PbTiO_3$, $BaTiO_3$, $CaZrO_3$, $SrZrO_3$, $PbZrO_3$ and $BaZrO_3$ perovskites all have a general chemical formula ABO_3, where (A = Ca, Sr, Pb or Ba and B = Ti or Zr). The A cation size as a rule is much larger than the relevant B cation size. The ABO_3 perovskite cubic-symmetry structure has the B atom in sixfold oxygen coordination, surrounded by an octahedron of O atoms as well as the A atom in 12-fold oxygen cuboctahedral coordination. As temperature

Address correspondence to E-mail: rieglitis@gmail.com

https://doi.org/10.1007/s10853-019-04016-3

decreases, some of ABO_3 perovskites, like $SrTiO_3$ and $BaZrO_3$, stay in its high-temperature cubic phase, while other ABO_3 perovskites, such as $CaTiO_3$, $PbTiO_3$, $BaTiO_3$, $CaZrO_3$, $SrZrO_3$ and $PbZrO_3$, exhibit different phase transitions. The neutral (001) as well as polar and charged (011) surfaces of the ABO_3 perovskites are both of fundamental interest for basic research, and also very important for practical applications, for example, numerous microelectronic, catalytic, and other high-technology applications as well as they are frequently used as substrates for growth of other materials such as cuprate superconductors [28–34].

The predictive power of ab initio calculations caused by both the explosive development of new computational codes and powerful increase in computer speed allows for us to design a new material for high technology purposes on the paper. Very good example is prediction of the average battery voltage for a large amount of 4 V battery cathodes from ab initio calculations by Ceder et al. [35, 36]. Moreover, on the basis of our ab initio calculations performed by Eglitis and Borstel [37, 38], it was demonstrated that the cubic spinel structure $Li_2CoMn_3O_8$ battery cathode material will lead to the novel high-voltage lithium-ion battery working at the 5 V range [37, 38].

A great variety of metal ions can occupy the A and B sites in the technologically important ABO_3 perovskite structure, and such versatility of this class of materials makes them a perfect choice for a large number of catalytic applications, including electrocatalytic operations. An SOEC cathode should have high electronic and ionic conductivities. An ABO_3 perovskite oxide can possess both of these conductivities. Thereby, very novel and forefront research direction is perovskite material cathodes. Due to the problems such as Ni reoxidation and requirement of using a reducing agent in the feed stream, coke deposition at lower temperatures, and further reduction of CO to carbon at high cathodic potentials, the focus of research on CO_2 electrolysis has shifted from improvement of metal-cermet electrodes to developing of alternative materials. Oxide-based mixed ionic and electrical conductors (MIECs), specifically perovskite-type MIEC oxides, have attracted attention due to their easily tunable ionic and electrical conductivity, high stability at high temperatures as well as resistance to coke formation.

Therefore, it is self-evident that in last 25 years $CaTiO_3$, $SrTiO_3$, $PbTiO_3$, $BaTiO_3$, $CaZrO_3$, $SrZrO_3$, $PbZrO_3$ and $BaZrO_3$ perovskite neutral (001) surfaces were world wide extensively explored both theoretically and experimentally [39–54]. Recently, systematic trends in ab initio calculations for eight technologically most important ABO_3 perovskite neutral (001) surfaces were summarized by Eglitis et al. [55, 56]. For example, it was pointed out that relaxation of ABO_3 perovskite (001) surface metal atoms for upper two surface layers, as a rule, is larger than that of oxygen atoms. For ABO_3 perovskite (001) surfaces, in most cases, all atoms of the first surface layer relax inwards, towards the bulk, all atoms of the second surface layer relax outwards, and, again, all atoms of the third surface layer relax inwards [55, 56]. It is worth to notice that for both AO and BO_2 terminations, the ABO_3 perovskite (001) surface energies are almost equivalent. According to our ab initio calculations [55, 56], the ABO_3 perovskite (001) surface band gaps are always reduced regarding to their respective bulk band gap values. Finally, in ABO_3 perovskite bulk, the B–O chemical bond population is always smaller than near the (001) surface [55, 56].

In contrast to neutral (001) surfaces, the ABO_3 perovskite polar (011) surfaces are much more complicated, since they consist of charged and polar planes, and thereby also of course less studied, both theoretically and experimentally. To the best of our knowledge, first ab initio study of the atomic and electronic structure of the polar $CaTiO_3$ (011) surface was performed by Zhang et al. [57]. The calculation results by Zhang et al. indicated that the energetically most favourable $CaTiO_3$ surfaces are the CaO-terminated (001) (0.824 eV), the A-type O-terminated (011) (0.837 eV), and the TiO_2-terminated (001) (1.021 eV) surfaces. This result by Zhang et al. [57] sharply contrasted with all another calculation results dealing with ABO_3 perovskite (001) and (011) surfaces [58–69], where the ABO_3 perovskite (001) surface energies are always smaller than (011) surface energies. One year later, Eglitis and Vanderbilt [11] performed very comprehensive first-principles calculations for three possible $CaTiO_3$ (011) surface terminations. Just opposite to Zhang et al. [57], Eglitis and Vanderbilt [11] found that CaO (0.94 eV)- and TiO_2 (1.13 eV)-terminated (001) surface energies are considerably smaller than the O-terminated (1.86 eV) $CaTiO_3$ (011) surface energy, in a line with all other

previous ab initio studies for ABO_3 perovskite polar (011) surfaces [58–69].

The first ab initio calculations for polar $SrTiO_3$ (011) surfaces were carried out by Bottin et al. [59]. One year later, Heifets and his co-workers [60] performed ab initio Hartree–Fock (HF) calculations for $SrTiO_3$ (011) surfaces. Around 10 years ago Eglitis and Vanderbilt [10] performed first-principles calculations for O-, Sr- and TiO-terminated $SrTiO_3$ (011) surfaces using a hybrid description of exchange and correlation. Finally, Enterkin et al. [61] reported a comprehensive research on the 3×1 polar $SrTiO_3$ (110) surface structure obtained through transmission electron diffraction and direct methods and confirmed through density functional theory calculations and scanning tunnelling microscopy images and simulations.

First in the world ab initio calculations for $PbTiO_3$ and $BaTiO_3$ (011) surfaces were performed by Eglitis and Vanderbilt [9]. Eglitis and Vanderbilt presented and discussed the results of calculations of surface relaxations and rumplings for the polar (011) surfaces of $PbTiO_3$ and $BaTiO_3$ by means of the hybrid B3PW description of exchange and correlation [9]. They considered three types of polar $PbTiO_3$ and $BaTiO_3$ (011) surfaces, terminated on a TiO layer, a Pb or Ba layer as well as O layer. They found that the relaxation energies for TiO-terminated $PbTiO_3$ and $BaTiO_3$ polar (011) surfaces are much larger than for the Pb- or Ba-terminated (011) surfaces. Two years later Zhang et al. [62] performed ab initio calculations of the atomic and electronic structure as well as stability of the polar $PbTiO_3$ (011) surfaces. At the same time independently Zhang et al. [63] by means of the GGA exchange–correlation functional performed first-principles calculations for the surface energy, cleavage energy, surface grand potential as well as surface relaxation for five different terminations of polar $PbTiO_3$ (011) surface. Simultaneously with Eglitis and Vanderbilt [9] in 2007, Xie et al. [64] investigated the electronic and atomic structures of the polar $BaTiO_3$ (011) surfaces by means of ab initio DFT calculations using the slab model. Finally, Wang et al. [65] explored the thermodynamic surface stability for polar $BaTiO_3$ (011) surface five terminations, namely BaTiO, TiO, Ba, O_2 and O.

To the best of our knowledge no ab initio studies exist dealing with polar $CaZrO_3$ (011) surfaces, and thereby in this paper we performed first in the world predictive theoretical calculations for $CaZrO_3$ (011) surfaces. Eglitis and Rohlfing [66] performed first ab initio calculations of surface relaxations, energetics, rumplings, optical band gaps as well as charge distribution for three different terminations of polar $SrZrO_3$ and $PbZrO_3$ (011) surfaces. It is worth to notice, that 4 years latter Chen et al. [67] also at ab initio level investigated the stabilities and electronic properties of five possible terminations for $SrZrO_3$ (011) polar surfaces.

First ab initio calculations for $BaZrO_3$ (011) surfaces were simultaneously performed 10 years ago by Eglitis [68] as well as by Heifets et al. [69]. Eglitis [68] performed polar $BaZrO_3$ (011) surface relaxation as well as calculated the surface energies and rumplings for three different terminations, namely Ba, ZrO and O. Heifets et al. [69] by means of the density functional theory calculations studied the atomic and electronic structure as well as charge redistribution of polar $BaZrO_3$ (011) surfaces.

Along with theoretical ab initio investigations of ABO_3 perovskite (011) surfaces, their polar (011) surfaces are world wide extensively studied also experimentally. For example, Crosby et al. [70] resolved the surface structure of (110) faceted strontium titanate nanoparticles synthesized via solvothermal method using high-resolution microscopy. The authors demonstrate that the surface is a titania-rich structure containing tetrahedrally coordinated TiO_4 units similar to the family of $(n \times 1)$ reconstructions observed on (110) surfaces of bulk crystalline $SrTiO_3$ [70]. As an another example of brilliant experimental work, 8 years ago Enterkin et al. [61] reported a solution to the 3×1 $SrTiO_3$ (110) surface structure obtained through transmission electron diffraction and direct methods and confirmed through scanning tunnelling microscopy and simulations [61].

The aim of this research paper was to carry out first in the world ab initio calculations for $CaZrO_3$ polar (011) surfaces in order to complete our more than 10 year long work dealing with first-principles calculations of polar and charged ABO_3 perovskite (011) surfaces [9–11, 59, 60, 66, 68]. For our $CaZrO_3$ (011) surface calculations, we chose the high symmetry cubic phase because it is most extensively studied for $CaTiO_3$, $SrTiO_3$, $PbTiO_3$, $BaTiO_3$, $SrZrO_3$, $PbZrO_3$ and $BaZrO_3$ perovskites. The (011) surface studies for other $CaZrO_3$ low symmetry phases remain a challenging problem for our future calculations. After we completed first-principles calculations for $CaZrO_3$

(011) surfaces, we analysed results for all eight ABO_3 perovskites, and detected systematic trends common for $CaTiO_3$, $SrTiO_3$, $PbTiO_3$, $BaTiO_3$, $CaZrO_3$, $SrZrO_3$, $PbZrO_3$ and $BaZrO_3$ perovskite polar (011) surfaces in a form interesting for a large audience of readers.

Computational method as well as polar $CaZrO_3$ (011) surface models and energies

In this paper, we performed ab initio calculations for polar $CaZrO_3$ (011) surfaces, using the hybrid exchange–correlation functional B3LYP [71] as well as the world well-known CRYSTAL [72] computer code. Our previous calculation results for $CaTiO_3$, $SrTiO_3$, $PbTiO_3$, $BaTiO_3$, $SrZrO_3$, $PbZrO_3$ and $BaZrO_3$ (011) surfaces performed by B3LYP [71] or B3PW [73] functional are listed for comparison purpose with aim to detect systematic trends in polar (011) surface calculations for all eight technologically most important ABO_3 perovskites. For $CaZrO_3$ bulk, we performed the reciprocal-space integration by sampling the Brillouin zone with an $8 \times 8 \times 8$ times, whereas for (011) surfaces with $8 \times 8 \times 1$ times extended Pack–Monkhorst net [74]. In this paper, for Ca, Zr and O atoms, we used exactly the same basis sets as in our previous work dealing with ab initio calculations of neutral $CaZrO_3$ (001) surfaces [75]. The polar $CaZrO_3$ (011) surfaces were modelled with two-dimensional (2D) slabs, which contained nine planes perpendicular to the [011] crystal direction (Fig. 1). The main difficulty in modelling the $CaZrO_3$ (011) polar surface is that it consists of charged planes, O–O or $CaZrO_3$. If we assume fixed ionic charges Ca^{2+}, Zr^{4+} and O^{2-} in the $CaZrO_3$ perovskite, then calculating the polar $CaZrO_3$ (011) surface precisely as would be acquired from a $CaZrO_3$ crystal cleavage leads to either an endless macroscopic dipole moment in the direction perpendicular to the (011) surface, when the slab is terminated by different planes—O_2 and CaZrO (Fig. 2a), or an excess of charge, when both sides of the slab are terminated by the same crystalline planes (O_2–O_2) (Fig. 2b) or (CaZrO–CaZrO) (Fig. 2c). It is well known that these two kinds of crystal terminations make the polar $CaZrO_3$ (011) surface unstable [1, 60, 76]. In ab initio calculations for a slab terminated by the different kind of planes the charge redistribution near the surface, in principle, can

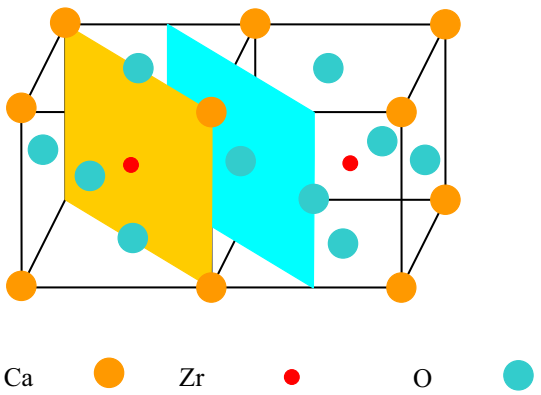

Figure 1 Schematic picture of the cubic $CaZrO_3$ perovskite structure containing two (011) cleavage planes which create charged O_2 and CaZrO (011) surfaces.

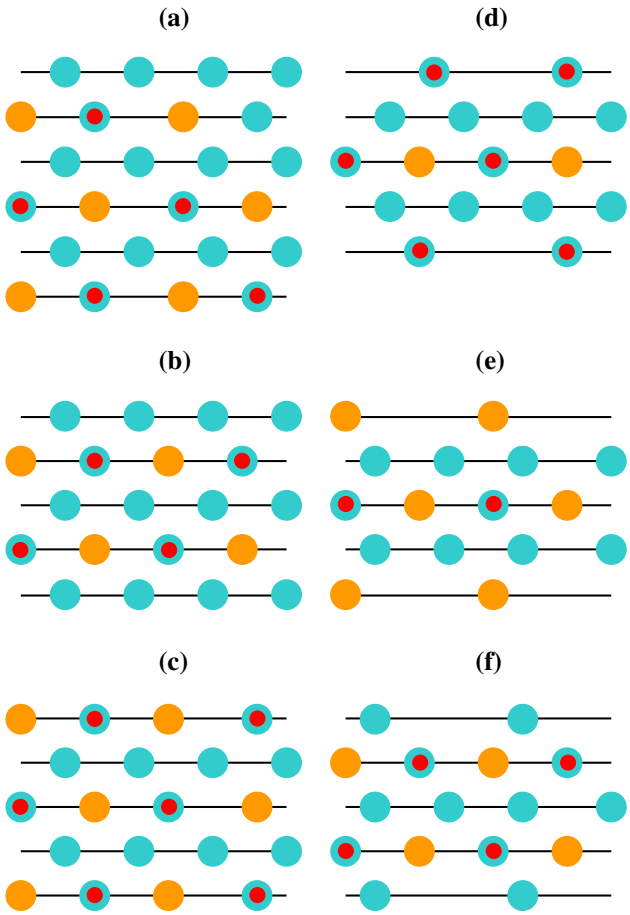

Figure 2 $CaZrO_3$ (011) surface slab models (**a**–**f**) used in our calculations. $CaZrO_3$ slabs obtained by crystal cleaving yields mixed O_2- and CaZrO-terminated polar surfaces (**a**), O_2-terminated (**b**) as well as CaZrO-terminated (**c**) charged surfaces. Our modified nonpolar and neutral TiO-terminated $CaZrO_3$ (011) surfaces (**d**), Ca-terminated (**e**) and O-terminated (**f**) surfaces.

compensate the macroscopic dipole moment. From another side, in the ab initio calculations of slabs terminated by the same planes the charge neutrality may be easily retained by setting in the computer input files an appropriate number of electrons or the zero net charge of the unit cell. Nevertheless, careful calculations [1, 59, 77] demonstrate that these two options for ABO_3 perovskite surfaces are energetically expensive with respect to the dipole moment elimination via introduction of vacancies.

For these two reasons, in order to get as good as possible results, we used for our $CaZrO_3$ (011) surface calculations nonpolar CaZrO-terminated surfaces and modified their upper and lower layers. Namely, we removed the Ca atom from the upper and lower layer of the nine-layer symmetric CaZrO-terminated slab (Fig. 2d). We get a neutral 21-atom containing ZrO-terminated $CaZrO_3$ (011) slab as illustrated in Fig. 2d. If we simultaneously remove both the Zr and O atoms from the upper and lower layers of the symmetric 9-layer CaZrO-terminated $CaZrO_3$ (011) slab, we get a neutral Ca-terminated $CaZrO_3$ (011) 9-layer slab which contains 19 atoms (Fig. 2e). Lastly, if we remove the O atom again from the upper and lower layers of the nine-layer symmetric O–O-terminated $CaZrO_3$ (011) slab, we get the neutral and symmetric 20-atom containing nine-layer supercell with O-terminated $CaZrO_3$ (011) surfaces (Fig. 2f).

With aim to calculate the $CaZrO_3$ (011) surface energies, we started with the cleavage energy calculations for unrelaxed Ca- and ZrO-terminated (011) surfaces. Surfaces with Ca and ZrO terminations simultaneously arise under (011) cleavage of the $CaZrO_3$ crystal. We assume that the cleavage energy is equally distributed between the created Ca- and ZrO-terminated (011) surfaces. In our $CaZrO_3$ (011) surface calculations, the nine-layer Ca-terminated (011) slab with 19 atoms and the ZrO-terminated (011) slab with 21 atoms together contain 40 atoms, or in another words eight bulk unit cells (40 atoms), thereby:

$$E^{\mathrm{unr}}_{\mathrm{surf}}(\Psi) = 1/4\left[E^{\mathrm{unr}}_{\mathrm{slab}}(\mathrm{Ca}) + E^{\mathrm{unr}}_{\mathrm{slab}}(\mathrm{ZrO}) - 8E_{\mathrm{bulk}}\right], \quad (1)$$

where Ψ means Ca or ZrO termination of $CaZrO_3$ (011) surface, $E^{\mathrm{unr}}_{\mathrm{slab}}(\Psi)$ are the total energies of the unrelaxed Ca- or ZrO-terminated $CaZrO_3$ (011) slabs, E_{bulk} is the total energy per bulk unit cell, and the coefficient of ¼ comes from the event that we create four surfaces due the cleavage procedure. As a next step, we will calculate the relaxation energies for each of Ca- and ZrO-terminated $CaZrO_3$ (011) slabs, when both sides of the slabs relax, by means of the following equation:

$$E_{\mathrm{rel}}(\Psi) = 1/2[E^{\mathrm{rel}}_{\mathrm{slab}}(\Psi) - E^{\mathrm{unr}}_{\mathrm{slab}}(\Psi)], \quad (2)$$

where $E^{\mathrm{rel}}_{\mathrm{slab}}(\Psi)$ is the slab energy after the geometry relaxation (Ψ = Ca or ZrO). The $CaZrO_3$ (011) surface energy is equal to a sum of the cleavage and relaxation energies:

$$E_{\mathrm{surf}}(\Psi) = E^{\mathrm{unr}}_{\mathrm{surf}}(\Psi) + E_{\mathrm{rel}}(\Psi), \quad (3)$$

Finally, in case when we cleave the $CaZrO_3$ crystal in another way, we got two equal O-terminated $CaZrO_3$ (011) surface slabs. Each of them contains 20 atoms. Thereby, we can simplify our calculations, since the unit cell of the nine-plane O-terminated $CaZrO_3$ (011) slab contains four bulk unit cells. The surface energy for O-terminated (011) surface is equal to:

$$E_{\mathrm{surf}}(\mathrm{O}) = 1/2\left[E^{\mathrm{rel}}_{\mathrm{slab}}(\mathrm{O}) - 4E_{\mathrm{bulk}}\right], \quad (4)$$

where $E_{\mathrm{surf}}(\mathrm{O})$ and $E^{\mathrm{rel}}_{\mathrm{slab}}(\mathrm{O})$ are the O-terminated $CaZrO_3$ (011) surface energy and the relaxed O-terminated $CaZrO_3$ (011) slab total energy.

Calculation results for polar $CaZrO_3$ (011) surfaces

As a first step of our calculations, we calculated, by means of the hybrid B3LYP functional, the $CaZrO_3$ bulk lattice constant and found it equal to 4.157 Å. In order to characterize the covalency effects and chemical bonding, we used a classical Mulliken population description for the effective atomic charges Q and other local properties of $CaZrO_3$ electronic structure as defined in Refs. [78, 79]. By means of B3LYP hybrid exchange–correlation functional, our calculated $CaZrO_3$ effective bulk atomic charges are equal to (+ 1.787e) for the Ca atom, (+ 2.144e) for the Zr atom, and (− 1.310e) for the O atom. Our calculated $CaZrO_3$ bulk bond population of the chemical bonding is largest between Zr and O atoms (+ 0.086e). The bond population between Ca and O atoms is more than six times smaller (+ 0.014e) than between Zr and O atoms. Finally, the bond population between O and O atoms is even negative (− 0.010e), which indicates a small repulsion between O and O atoms in the $CaZrO_3$ bulk matrix.

As we explained in "Computational method as well as polar $CaZrO_3$ (011) surface models and

energies" section, nonpolar and neutral ZrO-, Ca- and O-terminated (011) surfaces for the $CaZrO_3$ perovskite can be constructed by us as shown in Fig. 2d–f, respectively. Our calculated atomic displacements obtained by B3LYP hybrid exchange–correlation functional for ZrO-, Ca- and O-terminated $CaZrO_3$ (011) surfaces are shown in Table 1.

Table 1 Our B3LYP calculated atomic relaxations for the $CaZrO_3$ (011) surfaces (in per cent of the bulk lattice constant a_0) for the three surface terminations ZrO, Ca and O

Layer	Ion	Δz	Δy
ZrO-terminated $CaZrO_3$ (011) surface			
1	Zr	− 6.06	
1	O	+ 4.96	
2	O	− 0.38	
3	Ca	− 3.61	
3	O	− 7.94	
3	Zr	− 0.41	
Ca-terminated $CaZrO_3$ (011) surface			
1	Ca	− 18.67	
2	O	+ 1.25	
3	Zr	+ 0.25	
3	O	− 0.63	
3	Ca	− 0.14	
O-terminated $CaZrO_3$ (011) surface			
1	O	− 5.97	− 5.05
2	Zr	+ 0.75	− 2.17
2	Ca	+ 1.78	13.95
2	O	+ 0.67	1.32
3	O	+ 0.51	1.23

Positive signs correspond to outwards atomic displacements

From the results of our calculations (Table 1), all atoms of the upper $CaZrO_3$ (011) surface layer relax inward, namely towards the bulk, for all three ZrO-, Ca- and O-terminated $CaZrO_3$ (011) surfaces. The only exception is outward relaxation of ZrO-terminated $CaZrO_3$ (011) surface upper-layer O atom by 4.96% of the bulk lattice constant a_0. As we can see from Table 2 and Fig. 3, also for all another our calculated ABO_3 perovskites systematic trend is that all upper-layer atoms for all three (011) terminations relax inward with the exception of BO-terminated

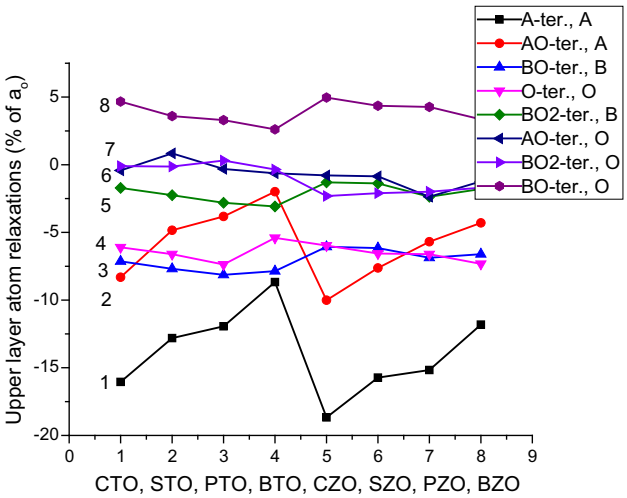

Figure 3 Our calculated upper-layer atom relaxations for all eight ABO_3 perovskite BO-, A- and O-terminated (011) as well as AO- and BO_2-terminated (001) surfaces. A-terminated (011) surface A atom relaxation (line 1). AO-terminated (001) surface A (line 2) and O (line 6) atom relaxations. BO-terminated (011) surface B atom (line 3) and O atom (line 8) atom relaxations. O-terminated (011) surface O atom relaxation (line 4). BO_2-terminated (001) surface B atom (line 5) and O atom (line 7) atom relaxations.

Table 2 Our calculated upper-layer atom relaxations for all eight ABO_3 perovskite AO-, A- and O-terminated (011) as well as AO- and BO_2-terminated (001) surfaces

Term	Atom	CTO	STO	PTO	BTO	CZO	SZO	PZO	BZO
BO (011)	B	− 7.14	− 7.69	− 8.13	− 7.86	− 6.06	− 6.16	− 6.87	− 6.61
	O	+ 4.67	+ 3.59	+ 3.30	+ 2.61	+ 4.96	+ 4.36	+ 4.27	+ 3.35
A (011)	A	− 16.05	− 12.81	− 11.94	− 8.67	− 18.67	− 15.73	− 15.17	− 11.81
O (011)	O	− 6.10	− 6.61	− 7.37	− 5.40	− 5.97	− 6.56	− 6.61	− 7.32
BO_2 (001)	B	− 1.71	− 2.25	− 2.81	− 3.08	− 1.30	− 1.38	− 2.37	− 1.79
	O	− 0.10	− 0.13	+ 0.31	− 0.35	− 2.31	− 2.10	− 1.99	− 1.70
AO (001)	A	− 8.31	− 4.84	− 3.82	− 1.99	− 10.01	− 7.63	− 5.69	− 4.30
	O	− 0.42	+ 0.84	− 0.31	− 0.63	− 0.79	− 0.86	− 2.37	− 1.23

Positive signs correspond to outwards atomic displacements

(011) surface upper-layer O atoms. The largest relaxation magnitude between all upper-layer $CaZrO_3$ (011) surface atoms exhibits the Ca-terminated (011) surface Ca atom by 18.67% of a_0. This our calculated Ca atom displacement magnitude (18.67% of a_0) is approximately three times larger than the relevant displacement magnitudes for Zr atom (6.06% of a_0) on the ZrO-terminated and O atom (5.97% of a_0) on the O-terminated $CaZrO_3$ polar (011) surfaces. Also for all another ABO_3 perovskites, the A atom inward relaxation magnitude on A-terminated (011) surface always is larger than the B atom and O atom relaxation magnitudes on BO- and O-terminated ABO_3 perovskite (011) surfaces (Table 2 and Fig. 3). However it is worth to notice that for the $BaTiO_3$ perovskite, the Ba atom inward relaxation (8.67% of a_0) on the Ba-terminated $BaTiO_3$ (011) surface is only slightly larger than the Ti atom inward relaxation (7.86% of a_0) on the TiO-terminated $BaTiO_3$ (011) surface (Table 2 and Fig. 3). As we can see from Table 2 and Fig. 3, systematic trend is that the ABO_3 perovskite (011) surface upper-layer atom relaxation almost always is larger than the (001) surface upper-layer atom relaxation. For ABO_3 perovskite (011) and (001) terminated surfaces, in most cases the metal atom relaxation magnitudes are larger than the oxygen atom relaxation magnitudes.

All second-layer ZrO-, Ca- and O-terminated $CaZrO_3$ (011) surface atoms relax upwards, with the sole exception for O atom on the ZrO-terminated (011) surface (Table 1). Such systematic tendency, mostly upward relaxation of second-layer atoms on BO-, A- and O-terminated (011) surfaces, is common for all eight ABO_3 perovskites (Table 3 and Fig. 4). Namely, according to our calculations, for CTO, STO, PTO, BTO, CZO, SZO, PZO and BZO perovskite second layers, upwards relax 23 atoms, whereas inwards only 17 atoms (Table 3 and Fig. 4).

Finally, all ZrO-, Ca- and O-terminated $CaZrO_3$ (011) surface third-layer atoms relax inwards, with the exception of Ca-terminated (011) surface third-layer Zr atom and O-terminated (011) surface O atom, which both relax upwards (Table 1). Also for all our eight calculated ABO_3 perovskite BO-, A- and O-terminated (011) surface third-layer atoms, a large majority, namely 37 atoms, relax inwards, while only 16 atoms relax outwards (Table 4 and Fig. 5).

According to our B3LYP calculations, on the ZrO-terminated $CaZrO_3$ (011) surface, the upper-layer Zr atom relax inwards by 6.06% of the a_0, but the same upper-layer O atom relax outwards by 4.96% (Table 1), creating a large surface rumpling equal to 11.02 (Table 5). On the ZrO-terminated $CaZrO_3$ (011) surface, the displacement magnitudes of all atoms in the third layer are larger than in the second-layer and the third-layer O atom displacement magnitude

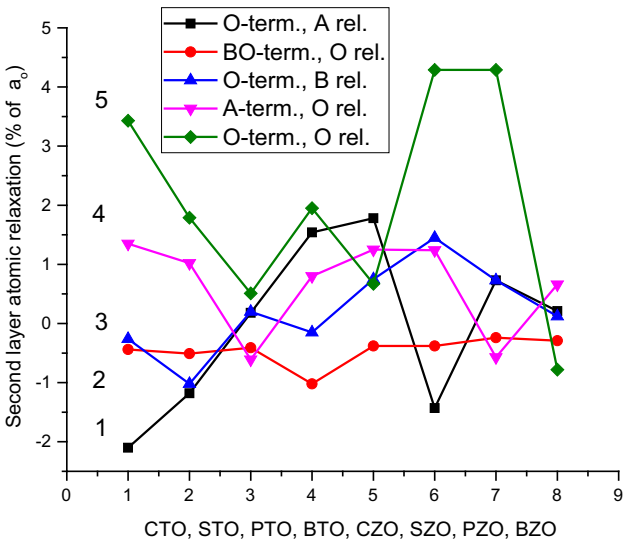

Figure 4 Our calculated O-terminated (011) surface A atom relaxations (line 1), BO-terminated (011) surface O atom relaxations (line 2), O-terminated (011) surface B atom relaxations (line 3), A-terminated (011) surface O atom relaxations (line 4), and, finally, O-terminated (011) surface O-atom relaxations (line 5).

Table 3 Our calculated second-layer atom relaxations for all eight ABO_3 perovskite BO-, A- and O-terminated (011) surfaces

Term	Atom	CTO	STO	PTO	BTO	CZO	SZO	PZO	BZO
BO (011)	O	− 0.44	− 0.51	− 0.41	− 1.02	− 0.38	− 0.38	− 0.24	− 0.29
A (011)	O	+ 1.35	+ 1.02	− 0.61	+ 0.80	+ 1.25	+ 1.24	− 0.57	+ 0.66
O (011)	B	− 0.26	− 1.02	+ 0.20	− 0.15	+ 0.75	+ 1.45	+ 0.73	+ 0.12
	A	− 2.10	− 1.18	+ 0.18	+ 1.54	+ 1.78	− 1.43	+ 0.73	+ 0.21
	O	+ 3.43	+ 1.79	+ 0.51	+ 1.95	+ 0.67	+ 4.29	+ 4.29	− 0.78

Positive signs correspond to outwards atomic displacements

Table 4 Our calculated third-layer atom relaxations for all eight ABO_3 perovskite AO-, A- and O-terminated (011) surfaces

Term	Atom	CTO	STO	PTO	BTO	CZO	SZO	PZO	BZO
BO (011)	B	− 0.78	+ 0.16	+ 0.30		− 0.41	− 0.40	− 0.02	+ 0.90
	A	− 2.75	− 2.10	− 2.54	− 0.88	− 3.61	− 1.94	− 2.37	− 1.51
	O	− 3.79	− 2.56	− 4.07		− 7.94	− 5.69	− 5.69	− 3.54
A (011)	B	− 0.37	− 0.04	+ 1.78	+ 0.16	+ 0.25	+ 0.10	− 0.66	+ 0.09
	A	− 0.93	+ 0.26	+ 1.52		− 0.14	− 0.48	+ 3.41	+ 0.71
	O	− 1.71	− 1.08	+ 1.67	− 0.43	− 0.63	− 0.95	+ 2.37	− 0.07
O (011)	O	− 0.55	− 0.79	− 0.41	+ 0.90	+ 0.51	− 0.10	− 0.19	− 0.07

Positive signs correspond to outwards atomic displacements

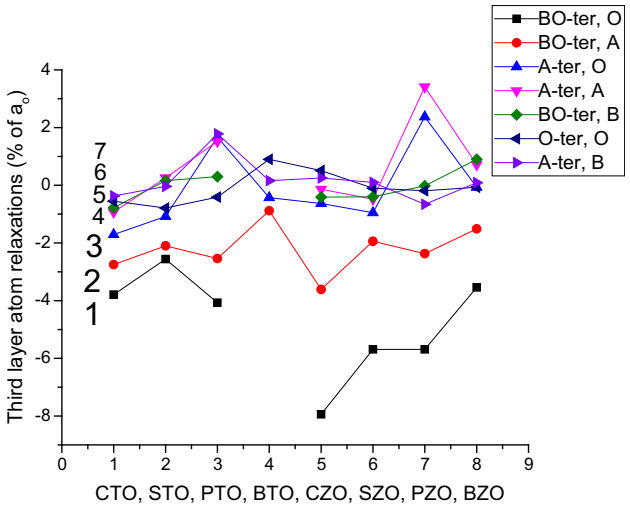

Figure 5 Our calculated third-layer atom relaxations for all eight ABO_3 perovskite BO, A and O-terminated (011) surfaces. BO-terminated (011) surface O atom relaxation (line 1), A atom relaxation (line 2) and B atom relaxation (line 5). A-terminated (011) surface O atom relaxation (line 3), A atom relaxation (line 4) and B atom relaxation (line 7) as well as O-terminated (011) surface O atom relaxation (line 6).

7.94% of a_0 is the largest displacement magnitude between ZrO-terminated (011) surface all three layer atoms (Table 1). Our calculated first interlayer distance Δd_{12} values (Table 5) show that the reduced distance between the first and second layers for ZrO-terminated $CaZrO_3$ (011) surface is more than 189 times larger than the corresponding expansion Δd_{23} between the second and third layers. From Table 5, all our eight calculated ABO_3 perovskite BO-terminated (011) surfaces exhibit very large surface rumpling, ranging from 9.96 for $BaZrO_3$ till 11.81 for $CaTiO_3$. For all our eight calculated ABO_3 perovskites, systematic trend is reduction in the interlayer distance Δd_{12}, ranging from 5.68 for $CaZrO_3$ till 7.72 for $PbTiO_3$. Our calculated BO-terminated (011) surface interlayer distance Δd_{23} is reduced for STO, PTO, BTO, PZO and BZO perovskites, but expanded by a very small magnitude for CZO, CTO and SZO perovskites (Table 5).

The O-terminated $CaZrO_3$ (011) surface has a lower symmetry than the ZrO- and Ca-terminated $CaZrO_3$ (011) surfaces; therefore, atomic displacements occur not only in the z direction perpendicular to the surface, but also in the y direction along the surface. For example, the O atom on the O-terminated $CaZrO_3$ (011) surface moves inwards, in the z direction by 5.97% and by a comparable magnitude of 5.05% also along the surface in the y direction (Table 1). All second-layer O-terminated $CaZrO_3$ (011) surface,

Table 5 Our calculated surface rumpling s and relative displacements Δd_{ij} (in per cent of the ABO_3 perovskite bulk lattice constant a_0) for the three near-surface planes on the BO- and O-terminated ABO_3 perovskite (011) surfaces

Material	BO-terminated (011) surface			O-terminated (011) surface	
	s	Δd_{12}	Δd_{23}	Δd_{12}	Δd_{23}
$CaZrO_3$ (this paper)	11.02	− 5.68	0.03	− 6.72	0.24
$CaTiO_3$ [11]	11.81	− 6.70	0.34	− 5.84	0.29
$SrTiO_3$ [10]	11.28	− 7.18	− 0.67	− 5.59	− 0.23
$PbTiO_3$ [9]	11.43	− 7.72	− 0.71	− 7.57	0.61
$BaTiO_3$ [9]	10.47	− 6.84	− 1.02	− 5.25	− 1.05
$SrZrO_3$ [62]	10.52	− 5.78	0.02	− 8.01	1.55
$PbZrO_3$ [62]	11.14	− 6.63	− 0.22	− 7.34	0.92
$BaZrO_3$ [64]	9.96	− 6.32	− 1.19	− 7.44	0.19

atoms relax outwards in the z direction by 0.75% for Zr atom, 1.78% for Ca atom and 0.67% for O atom. It is worth to notice that the second-layer Ca atom exhibits the largest displacement magnitude among all our calculated $CaZrO_3$ atoms along the surface in the y direction by 13.95%. The third-layer O atom, same as all three second-layer atoms, also moves outward in the z direction, but by a small displacement magnitude of 0.51%. From Table 5, for the O-terminated $CaZrO_3$ (011) surface there is a substantial contraction of the interlayer distance Δd_{12} on the z direction by 6.72% and only a very small expansion of Δd_{23} by 0.24%. Also for all other our calculated ABO_3 perovskites a large contraction of the interlayer distance Δd_{12} for O-terminated (011) surface occurs ranging from 5.25% for BTO till 8.01% for SZO. For most of ABO_3 perovskite O-terminated (011) surfaces, like CZO, CTO, PTO, SZO, PZO and BZO, there are a small expansion of the interlayer distance Δd_{23} observed from our calculations, whereas for STO and BTO perovskites the interlayer distance Δd_{23} contracts. Comparison of surface rumpling s and interlayer distances Δd_{ij} for ABO_3 perovskite (011) and (001) surfaces is depicted in Fig. 6. As we can see from Fig. 6, surface rumplings s for ABO_3 perovskite BO-terminated (011) surfaces are always larger than the relevant surface rumplings for AO and especially BO_2-terminated ABO_3 perovskite (001) surfaces. ABO_3 perovskite interlayer distances Δd_{12} are always reduced for their BO-terminated (011) as well as BO_2 and especially AO-terminated (001) surfaces (Fig. 6). In contrast, the interlayer distances Δd_{23} are always expanded for ABO_3 perovskite (001) surfaces, but they may be either expanded or reduced for BO- and O-terminated (011) surfaces (Fig. 6).

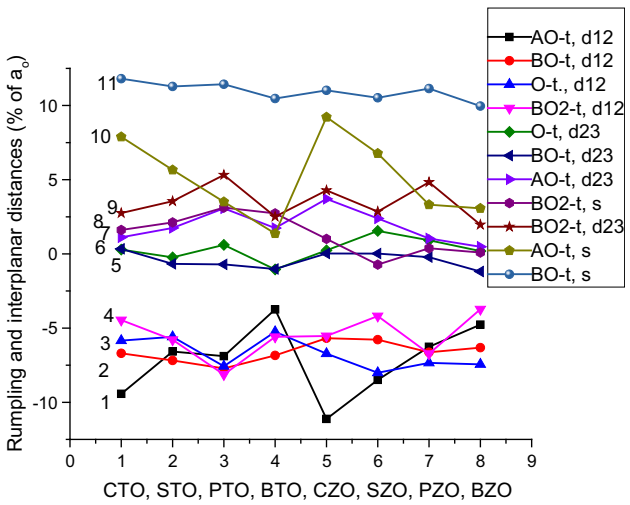

Figure 6 Our calculated surface rumplings s and interplanar distances Δd_{12} and Δd_{23} for BO (lines 2, 6, 11)- and O (lines 3, 5)-terminated ABO_3 perovskite polar (011) surfaces as well as for BO_2 (lines 4, 8, 9)- and AO (lines 1, 7, 10)-terminated neutral (001) surfaces.

Our calculated surface energies of the relaxed ZrO-, Ca- and O-terminated $CaZrO_3$ (011) surfaces are presented in Table 6 and plotted in Fig. 7 together with another ABO_3 perovskite (011) as well as for comparison purpose also BO_2- and AO-terminated ABO_3 perovskite (001) surface energies [55]. The $CaZrO_3$ (011) surface energies were computed by us using Eqs. (1)–(4). Unlike the ABO_3 perovskite (001) surfaces [55], from Table 6 we can see that different terminations of the ABO_3 perovskite (011) surface, as a rule, lead to considerable difference in the surface energies. For example, the our calculated surface energy difference between ZrO (3.46 eV)- and Ca (1.49 eV)-terminated $CaZrO_3$ (011) surfaces is really huge and equal to 1.97 eV, which is more than any of ZrO_2 (1.33 eV)- or CaO (0.87 eV)-terminated $CaZrO_3$ (001) surface energies. Among all three of our B3LYP calculated $CaZrO_3$ (011) surfaces, the Ca-terminated $CaZrO_3$ (011) surface has the lowest surface energy

Table 6 Our calculated surface energies for $CaZrO_3$, $CaTiO_3$ [11], $SrTiO_3$ [10], $PbTiO_3$ [9], $BaTiO_3$ [9], $SrZrO_3$ [66], $PbZrO_3$ [66] and $BaZrO_3$ [68] (011) surfaces (in electron volt per surface cell). Our earlier calculated ABO_3 perovskite (001) surface energies are listed for comparison purpose [9–11, 66, 68, 75]

Term	E_{surf}	CTO	STO	PTO	BTO	CZO	SZO	PZO	BZO
BO	(011)	3.13	3.06	1.36	2.04	3.46	3.61	1.89	3.09
A	(011)	1.91	2.66	2.03	3.24	1.49	2.21	1.74	2.90
O	(011)	1.86	2.04	1.72	1.72	2.08	2.23	1.85	2.32
BO_2	(001)	1.13	1.23	0.74	1.07	1.33	1.24	0.93	1.31
AO	(001)	0.94	1.15	0.83	1.19	0.87	1.13	1.00	1.30

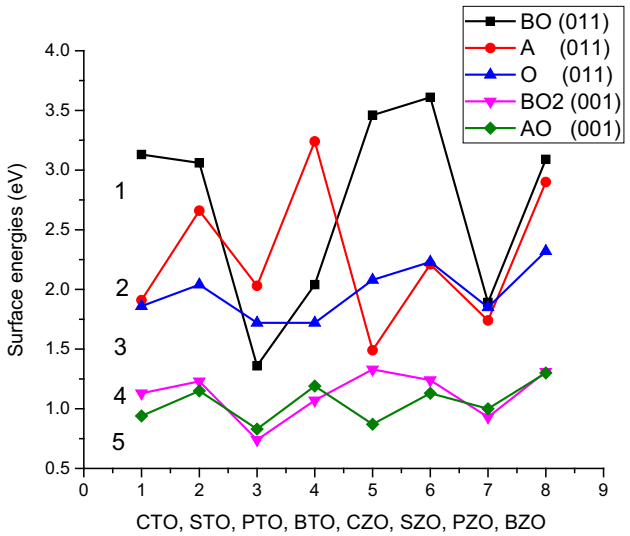

Figure 7 Our calculated ABO_3 perovskite surface energies for polar BO (line 1)-, A (line 2)- and O (line 3)-terminated (011) as well as neutral BO_2 (line 4)- and AO (line 5)-terminated (001) surfaces.

equal to 1.49 eV, which only slightly by 0.16 eV exceeds the surface energy for ZrO_2-terminated $CaZrO_3$ (001) surface [75]. The surface energy for the Ca-terminated $CaZrO_3$ (011) surface 1.49 eV is more than two times smaller than the ZrO-terminated $CaZrO_3$ (011) surface energy 3.46 eV (Table 6). The O-terminated $CaZrO_3$ (011) surface energy 2.08 eV is very close to the sum of ZrO_2 (1.33 eV)- and CaO (0.87 eV)-terminated $CaZrO_3$ (001) surface energies equal to 2.20 eV.

In Table 7, we collected our B3LYP calculated interatomic distances R as well as chemical bond populations P for the ZrO, Ca and O terminations of the $CaZrO_3$ (011) surface. The most important effect observed here is a strong increase in the Zr–O chemical bonding covalency near the ZrO- and O-terminated $CaZrO_3$ (011) surface as compared to both the $CaZrO_3$ bulk (0.086*e*) and even to the ZrO_2-terminated $CaZrO_3$ (001) surface 0.102*e*. For the O-terminated $CaZrO_3$ (011) surface, the O(I)–Zr(II) chemical bond population is equal to 0.130*e*, which is by 0.044*e* larger than the $CaZrO_3$ bulk Zr–O bond population as well as by 0.028*e* larger than the relevant ZrO_2-terminated $CaZrO_3$ (001) surface chemical bond population. For our calculated ZrO-terminated $CaZrO_3$ (011) surface, the Zr–O chemical bond population is larger in the direction perpendicular to the ZrO-terminated (011) surface 0.240*e* than in the plane 0.138*e* (Table 7). As we can see from Table 8 and

Table 7 Our calculated A–B chemical bond populations P (in *e*) as well as interatomic distances R (in Å) on $CaZrO_3$ (011) surfaces

$CaZrO_3$ (011) surface			
Atom *A*	Atom *B*	*P*	*R*
ZrO-terminated $CaZrO_3$ (011) surface			
Zr(I)	O(I)	0.138	2.128
	O(II)	0.240	1.919
O(II)	Zr(III)	0.114	2.079
	Ca(III)	0.018	3.009
	O(III)	0.012	3.108
Zr(III)	Ca(III)	0.002	3.603
	O(III)	0.114	2.102
	O(IV)	0.082	2.067
Ca(III)	O(III)	0.016	2.945
	O(IV)	0.016	2.867
O(III)	O(IV)	− 0.052	2.789
Ca-terminated $CaZrO_3$ (011) surface			
Ca(I)	O(II)	0.028	2.625
O(II)	Ca(III)	0.022	2.969
	Zr(III)	0.078	2.108
	O(III)	− 0.010	2.979
Ca(III)	O(III)	0.012	2.94
	O(IV)	0.014	2.936
Zr(III)	O(III)	0.052	2.079
	Ca(III)	0.002	3.600
	O(IV)	0.112	2.086
O(III)	O(IV)	− 0.012	2.927
O-terminated $CaZrO_3$ (011) surface			
O(I)	Ca(II)	0.022	2.470
	Zr(II)	0.130	1.986
	O(II)	− 0.010	2.959
Ca(II)	O(II)	− 0.012	2.415
	Zr(II)	− 0.002	3.078
Zr(II)	O(II)	0.084	2.084
	O(III)	0.186	1.989
O(II)	O(III)	− 0.002	2.945
Ca(II)	O(III)	0.006	2.743
O(III)	O(IV)	− 0.014	2.939
	Zr(IV)	0.066	2.130
	Ca(IV)	0.012	2.925

Symbols I–IV denote the number of each plane enumerated from the surface. The nearest-neighbour Zr–O distance is 2.0785 Å in $CaZrO_3$ bulk

Fig. 8, systematic trend is that the B–O chemical bond population in all our eight calculated ABO_3 perovskite bulk as a rule are smaller than near their (001) as well as especially (011) surfaces. It is worth to notice that for all eight ABO_3 perovskites (Table 8 and Fig. 8), the BO-terminated (011) surface B–O

Table 8 Our calculated eight ABO_3 perovskite bulk, BO_2-terminated (001) surface as well as BO-terminated (011) surface B–O chemical bond populations in the plane (B(I)–O(I)) and in the direction perpendicular to the (011) surface (B(I)–O(II))

	CZO	CTO	STO	PTO	BTO	SZO	PZO	BZO
Bulk (B–O)	0.086	0.084	0.088	0.098	0.098	0.092	0.106	0.108
(001) (B–O)	0.102	0.114	0.118	0.114	0.126	0.114	0.116	0.132
(011) (B(I)–O(I))	0.138	0.128	0.130	0.132	0.130	0.142	0.148	0.152
(011) (B(I)–O(II)	0.240	0.186	0.188	0.196	0.198	0.246	0.252	0.252

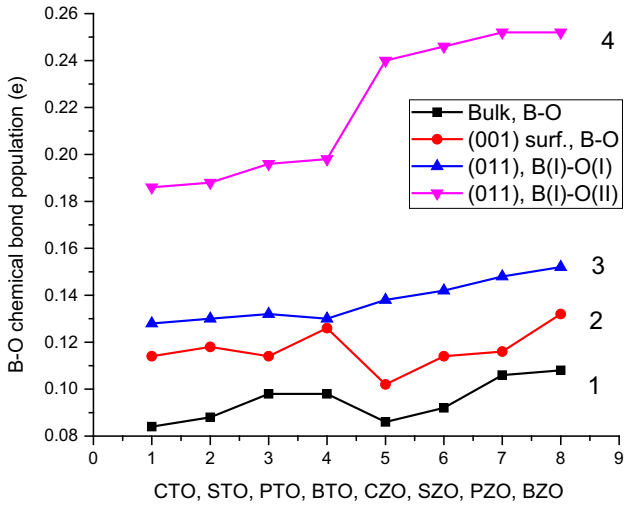

Figure 8 Our calculated B–O chemical bond populations for ABO_3 perovskite bulk (line 1), BO_2-terminated (001) surfaces (line 2) as well as B(I)–O(I) (line 3) and B(I)–O(II) (line 4) chemical bond populations for the BO-terminated ABO_3 perovskite (011) surfaces.

chemical bond population is larger in the direction perpendicular to the BO-terminated (011) surface than in the plane.

In Table 9 we listed our calculated $CaZrO_3$ effective Mulliken charges Q as well as their changes ΔQ in comparison with the respective bulk values for near the surface atoms for the ZrO-, Ca- and O-terminated $CaZrO_3$ (011) surfaces. Firstly, on the ZrO-terminated $CaZrO_3$ (011) surface, the effective Mulliken charge on the first surface layer Zr atom (+ 2.178*e*) is slightly increased by + 0.034*e* in comparison with the relevant bulk value. The third-layer metal atom Ca loses − 0.033*e* charge, while the other third-layer metal atom Zr gains almost the same amount of charge, namely 0.039*e*. It is interesting to notice that the O atoms in the first, second, third and fourth surface layers have reduced charges making them less negative. The largest O atom charge change equal to (0.178*e*) is observed for the $CaZrO_3$ subsurface O atoms, thereby giving a large positive charge

Table 9 Our B3LYP calculated Mulliken atomic charges Q (in *e*) and changes in atomic charges ΔQ with respect to the $CaZrO_3$ bulk charges (in *e*) on the ZrO-, Ca- and O-terminated $CaZrO_3$ (011) surfaces

$CaZrO_3$ (011) surface		
Atom	Q	ΔQ
ZrO-terminated $CaZrO_3$ (011) surface		
Zr(I)	+ 2.178	+ 0.034
O(I)	− 1.263	+ 0.047
O(II)	− 1.132	+ 0.178
Ca(III)	+ 1.754	− 0.033
Zr(III)	+ 2.183	+ 0.039
O(III)	− 1.283	+ 0.027
O(IV)	− 1.300	+ 0.01
Ca-terminated $CaZrO_3$ (011) surface		
Ca(I)	+ 1.686	− 0.101
O(II)	− 1.467	− 0.157
Ca(III)	+ 1.778	− 0.009
Zr(III)	+ 2.177	+ 0.033
O(III)	− 1.394	− 0.084
O(IV)	− 1.312	− 0.002
O-terminated $CaZrO_3$ (011) surface		
O(I)	− 1.314	− 0.004
Ca(II)	+ 1.734	− 0.053
Zr(II)	+ 2.173	+ 0.029
O(II)	− 1.327	− 0.017
O(III)	− 1.297	+ 0.013
Ca(IV)	+ 1.775	− 0.012
Zr(IV)	+ 2.153	+ 0.009
O(IV)	− 1.291	+ 0.019

The $CaZrO_3$ bulk Mulliken charges are equal to 1.787*e* for Ca, 2.144*e* for Zr, and − 1.310*e* for O

change of 0.356*e* for the whole subsurface layer (Table 9).

On the $CaZrO_3$ Ca-terminated (011) surface, the only positive charge change is observed for the third-layer Zr atom, where the Zr atom charge increases by 0.033*e* from the bulk value 2.144*e* till 2.177*e*. The largest charge changes are for the subsurface O ion (0.157*e*) as well as surface Ca ion (0.101*e*). Thereby,

our calculated largest overall charge change occurs in the Ca-terminated $CaZrO_3$ (011) surface subsurface layer (0.314*e*). On the O-terminated $CaZrO_3$ (011) surface, the largest charge change between all atoms is observed for the subsurface Ca atom equal to 0.053*e*, whereas the total charge density change in the fourth layer is almost negligible and equal to only 0.016*e*.

Summary and conclusions

Based on our current ab initio B3LYP calculations for polar $CaZrO_3$ (011) surfaces as well as for comparison purposes listed previous B3PW and B3LYP calculations [9–11, 66, 68, 75] for CTO, STO, PTO, BTO, SZO, PZO and BZO (011) surfaces, the following systematic trends for ABO_3 perovskite polar (011) surfaces were detected:

1. For ABO_3 perovskite polar (011) surfaces, systematic trend is that most of upper-layer atoms relax inwards, with only exception of all eight ABO_3 perovskite BO-terminated (011) surface O atoms. Twenty three of BO-, A- and O-terminated ABO_3 perovskite (011) surface second-layer atoms relax outwards, whereas 17 second-layer atoms inwards. Finally, a large majority of (011) surface third-layer atoms, namely 37 atoms, relax inwards, while only 16 remaining atoms relax outwards. It is worth to notice, that inward relaxation of upper-layer atoms, upwards relaxation of second-layer atoms and, again, inwards relaxation of third-layer atoms were even more strongly pronounced effect for the ABO_3 perovskite (001) surfaces [55].
2. The strongest relaxation magnitude between all BO-, A-, and O-terminated ABO_3 perovskite (011) surfaces always exhibit the A-terminated (011) surface upper-layer A atoms. The BO-terminated ABO_3 perovskite (011) surface third-layer atoms, in most cases, exhibit larger relaxation magnitude than the second-layer atoms.
3. The BO-terminated ABO_3 perovskite (011) surface upper layer rather large metal atom inwards relaxation as well as the same upper-layer oxygen atom outwards relaxation leads to a considerable rumpling of the outermost plane ranging from 9.96 for BZO till 11.81 for CTO. For all our eight calculated ABO_3 perovskite BO and O-terminated (011) surfaces, a systematic trend is a strong contraction of the interlayer distance Δd_{12}, ranging from 5.68 (CZO) till 7.72 (PTO) for BO-terminated (011) surface as well as from 5.25 (BTO) till 8.01 (SZO) for O-terminated $CaZrO_3$ (011) surface. For all eight ABO_3 perovskites and for both BO and O terminations, the interlayer distance Δd_{23} exhibits either very small expansion for ZrO-terminated (011) surface for CZO, CTO, SZO perovskites ranging from 0.03 (CZO) till 0.34 (CTO) and for O-terminated (011) surfaces small expansion is observed for CZO, CTO, PTO, SZO, PZO and BZO ranging from 0.19 BZO till 1.55 (CZO), or a small contraction for remaining of eight ABO_3 perovskites.
4. Unlike the ABO_3 perovskite (001) surfaces [55] different BO, A and O terminations of the ABO_3 perovskite (011) surface, as a rule, usually, lead to a considerable difference in the surface energies. Our calculated eight ABO_3 perovskite (011) surface energies are always larger than the (001) surface energies. Although in some cases, the ABO_3 perovskite (011) and (001) surface energies are really close, as for example the $CaZrO_3$ perovskite Ca-terminated $CaZrO_3$ (011) surface energy (1.49 eV) only by 0.16 eV exceeds the ZrO_2-terminated $CaZrO_3$ (001) surface energy equal to 1.33 eV.
5. The B–O chemical bond population in ABO_3 perovskites increase in direction from the bulk, ranging from 0.084*e* (CTO) till 0.108*e* (BZO) towards the BO_2-terminated (001) surface, ranging from 0.102*e* (CZO) till 0.132*e* (BZO) and reach its maximum for BO-terminated ABO_3 perovskite (011) surface. Our calculated BO-terminated (011) surface B(I)–O(I) in plane chemical bond population is in the range from 0.128*e* (CTO) till 0.152*e* (BZO). Finally, the maximal chemical bond population value is for the direction perpendicular to the BO-terminated ABO_3 perovskite (011) surface, where B(I)–O(II) values are in the range from 0.186*e* (CTO) till 0.252*e* (PZO, BZO).

Acknowledgements

Financial support via Latvian-Ukrainian Joint Research Project No. LV-UA/2018/2 for A. I. Popov,

Latvian Council of Science Project No. 2018/2-0083 "Theoretical prediction of hybrid nanostructured photocatalytic materials for efficient water splitting" for R. I. Eglitis and J. Kleperis as well as ERAF project No. 1.1.1.1/18/A/073 for R. I. Eglitis and J. Purans is greatly acknowledged.

Compliance with ethical standards

Conflict of interest The authors declare that they have no conflict of interest.

References

[1] Noguera C (2000) Polar oxide surfaces. J Phys Condens Matter 12:R367–R410

[2] Goniakowski J, Finocchi F, Noguera C (2008) Polarity of oxide surfaces and nanostructures. Rep Prog Phys 71:016501

[3] Sanna S, Schmidt WG (2017) $LiNbO_3$ surfaces from a microscopic perspective. J Phys Condens Matter 29:413001

[4] Dawber M, Rabe KM, Scott JF (2005) Physics of thin-film ferroelectric oxides. Rev Mod Phys 77:1083–1130

[5] Ribeiro RAP, Andrés J, Longo E, Lazaro SR (2018) Magnetism and multiferroic properties at $MnTiO_3$ surfaces: a DFT study. Appl Surf Sci 452:463–472

[6] Ribeiro RAP, Lazaro SR, Gatti C (2016) The role of exchange–correlation functional on the description of multiferroic properties using density functional theory: the $ATiO_3$ (A = Mn, Fe, Ni) case study. RSC Adv 6:101216–101225

[7] Liu ZQ, Liu JH, Biegalski MD, Hu JM, Shang L, Ji Y, Wang JM, Hsu SL, Wong AT, Cordill MJ, Gludovatz B, Marker C, Yan H, Feng ZX, You L, Lin MW, Ward TZ, Liu ZK, Jiang CB, Chen LQ, Ritchie RO, Christen HM, Ramesh R (2018) Electrically reversible cracks in an intermetallic film controlled by an electric field. Nat Commun 9:41

[8] Cohen RE (1992) Origin of ferroelectricity in perovskite oxides. Nature 358:136–138

[9] Eglitis RI, Vanderbilt D (2007) Ab initio calculations of $BaTiO_3$ and $PbTiO_3$ (001) and (011) surface structure. Phys Rev B 76:155439

[10] Eglitis RI, Vanderbilt D (2008) First-principles calculations of atomic and electronic structure of $SrTiO_3$ (001) and (011) surfaces. Phys Rev B 77:195408

[11] Eglitis RI, Vanderbilt D (2008) Ab initio calculations of the atomic and electronic structure of $CaTiO_3$ (001) and (011) surfaces. Phys Rev B 78:155420

[12] Yukawa R, Ozawa K, Yamamoto S, Liu RY, Matsuda I (2015) Anisotropic effective mass approximation model to calculate multiple subband structures at wide-gap semiconductor surfaces: application to accumulation layers of $SrTiO_3$ and ZnO. Surf Sci 641:224–230

[13] Kronik L, Shapira Y (1999) Surface photovoltage phenomena: theory, experiment, and applications. Surf Sci Rep 37:1–206

[14] Zhu Y, Salvador PA, Rohrer GS (2017) Controlling the termination and photochemical reactivity of the $SrTiO_3$ (110) surface. Phys Chem Chem Phys 19:7910–7918

[15] Janesko BG, Jones SI (2017) Quantifying the delocalization of surface and bulk *F*-centers. Surf Sci 659:9–15

[16] Kotomin EA, Eglitis RI, Maier J, Heifets E (2001) Calculations of the atomic and electronic structure for $SrTiO_3$ perovskite thin films. Thin Solid Films 400:76–80

[17] Koirala P, Gulec A, Marks LD (2017) Surface heterogeneity in $KTaO_3$ (001). Surf Sci 657:15–19

[18] Piskunov S, Eglitis RI (2015) First principles hybrid DFT calculations of $BaTiO_3/SrTiO_3$ (001) interface. Solid State Ion 274:29–33

[19] Carrasco J, Illas F, Lopez N, Kotomin EA, Zhukovskii YF, Evarestov RA, Mastrikov YA, Piskunov S, Maier J (2006) First-principles calculations of the atomic and electronic structure of *F* centers in the bulk and on the (001) surface of $SrTiO_3$. Phys Rev B 73:064106

[20] Li D, Zhao MH, Garra J, Kolpak AM, Rappe AM, Bonnell DA, Vohs JM (2008) Direct in situ determination of the polarization dependence of physisorption on ferroelectric surfaces. Nat Mater 7:473–477

[21] Fong DD, Kolpak AM, Eastman JA, Streiffer SK, Fuoss PH, Stephenson GB, Thompson C, Kim DM, Choi KJ, Eom CB, Grinberg I, Rappe AM (2006) Stabilization of monodomain polarization in ultrathin $PbTiO_3$ films. Phys Rev Lett 96:127601

[22] Eglitis RI, Piskunov S, Zhukovskii YF (2016) Ab initio calculations of $PbTiO_3/SrTiO_3$ (001) heterostructures. Phys Status Solidi C 13:913–920

[23] Kolpak AM, Li D, Shao R, Rappe AM, Bonnell DA (2008) Evolution of the structure and thermodynamic stability of the $BaTiO_3$ (001) surface. Phys Rev Lett 101:036102

[24] Piskunov S, Eglitis RI (2016) Comparative ab initio calculations of $SrTiO_3/BaTiO_3$ and $SrZrO_3/PbZrO_3$ (001) heterostructures. Nucl Instrum Methods Phys Res Sect B Beam Interact Mater Atoms 374:20–23

[25] Gerhold S, Riva M, Yildiz B, Schmid M, Diebold U (2016) Adjusting island density and morphology of the $SrTiO_3$ (110)-(4 × 1) surface: pulsed laser deposition combined with scanning tunnelling microscopy. Surf Sci 651:76–83

[26] Jia W, Vikhnin VS, Liu H, Kapphan S, Eglitis R, Usvyat D (1999) Critical effects in optical response due to charge transfer vibronic excitons and their structure in perovskite like systems. J Lumin 83–84:109–113

[27] Farlenkov AS, Ananyev MV, Eremin VA, Porotnikova NM, Kurumchin EK, Melekh BT (2016) Oxygen isotope exchange in doped calcium and barium zirconates. Solid State Ion 290:108–115
[28] Scott JF (2000) Ferroelectric memories. Springer, Berlin
[29] Lines ME, Glass AM (1977) Principles and applications of ferroelectrics and related materials. Clarendon, Oxford
[30] Anan'ev MV, Bershitskaya NM, Plaksin SV, Kurumchin EK (2012) Phase equilibriums, oxygen exchange kinetics and diffusion in oxides $CaZr_{1-x}Sc_xO_{3-x/2-\delta}$. Russ J Electrochem 48:879–886
[31] Antonova EP, Ananyev MV, Porotnikova NM, Kurumchin EK (2016) Oxygen isotope exchange and electrical conductivity of $CaZr_{1-x}Sc_xO_{3-x/2}$. J Solid State Electrochem 20:1497–1500
[32] Lyagaeva YG, Medvedev DA, Demin AK, Yaroslavtseva TV, Plaksin SV, Porotnikova NM (2014) Specific features of preparation of dense deramic based on barium zirconate. Semiconductors 48:1353–1358
[33] Savchin VP, Popov AI, Aksimentyeva OI, Klym H, Horbenko YY, Serga V, Moskina A, Karbovnyk I (2016) Cathodoluminescence characterization of polystyrene-$BaZrO_3$ hybrid composites. Low Temp Phys 42:760–763
[34] Aksimentyeva OI, Savchyn VP, Dyakonov VP, Piechota S, Horbenko YY, Opainych IY, Demchenko PY, Popov A, Szymczak H (2014) Modification of polymer-magnetic nanoparticles by luminescent and conducting substances. Mol Cryst Liq Cryst 590:35–42
[35] Ceder G (1998) Computational materials science—predicting properties from scratch. Science 280:1099–1100
[36] Ceder G, Chiang YM, Sadoway DR, Aydinol MK, Jang YI, Huang B (1998) Identification of cathode materials for lithium batteries guided by first-principles calculations. Nature 392:694–696
[37] Eglitis RI, Borstel G (2005) Towards a practical rechargeable 5 V Li ion battery. Phys Status Solidi A 202:R13–R15
[38] Eglitis RI (2015) Theoretical prediction of the 5 V rechargeable Li ion battery using $Li_2CoMn_3O_8$ as a cathode. Phys Scr 90:094012
[39] Arrigoni M, Kotomin EA, Maier J (2017) First-principles study of perovskite ultrathin films: stability and confinement effects. Isr J Chem 57:509–521
[40] Arrigoni M, Bjørnheim TS, Kotomin EA, Maier J (2016) First principles study of confinement effects for oxygen vacancies in $BaZrO_3$ (001) ultra-thin films. Phys Chem Chem Phys 18:9902–9908
[41] Iles N, Finocchi F, Khodja KD (2010) A systematic study of ideal and double layer reconstructions of ABO3 (001) surfaces (A = Sr, Ba; B = Ti, Zr). J Phys Condens Matter 22:305001
[42] Aballe L, Matencio S, Foerster M, Barrena E, Sanchez F, Fontcuberta J, Ocal C (2015) Instability and surface potential modulation of self-patterned (001) $SrTiO_3$ surfaces. Chem Mater 27:6198–6204
[43] Goh ES, Ong LH, Yoon TL, Chew KH (2016) Structural relaxation of $BaTiO_3$ slab with tetragonal (100) surface: ab-initio comparison of different thickness. Curr Appl Phys 16:1491–1497
[44] Eglitis RI (2015) Ab initio hybrid DFT calculations of $BaTiO_3$, $PbTiO_3$, $SrZrO_3$ and $PbZrO_3$ (111) surfaces. Appl Surf Sci 358:556–562
[45] Zhuang HL, Ganesh P, Cooper VR, Xu H, Kent PRC (2014) Understanding the interactions between oxygen vacancies at $SrTiO_3$ (001) surfaces. Phys Rev B 90:064106
[46] Borstel G, Eglitis RI, Kotomin EA, Heifets E (2003) Modelling of defects and surfaces in perovskite ferroelectrics. Phys Status Solidi B 236:253–264
[47] Lee YL, Morgan D (2015) Ab initio defect energetics of perovskite (001) surfaces for solid oxide fuel cells. A comparative study of $LaMnO_3$ versus $SrTiO_3$ and $LaAlO_3$. Phys Rev B 91:195430
[48] Luo B, Wang X, Tian E, Li G, Li L (2015) Structural and electronic properties of cubic $KNbO_3$ (001) surfaces: a first-principles study. Appl Surf Sci 351:558–564
[49] Eglitis RI (2013) Ab initio calculations of the atomic and electronic structure of $BaZrO_3$ (111) surfaces. Solid State Ion 230:43–47
[50] Brik MG, Ma CG, Krasnenko V (2013) First-principles calculations of the structural and electronic properties of the cubic $CaZrO_3$ (001) surfaces. Surf Sci 608:146–153
[51] Pilania G, Ramprasad R (2010) Adsorption of atomic oxygen on cubic $PbTiO_3$ and $LaMnO_3$ (001) surfaces: a density functional theory study. Surf Sci 604:1889–1893
[52] Cord B, Courths R (1985) Electronic study of $SrTiO_3$ (001) surfaces by photoemission. Surf Sci 162:34–38
[53] Dejneka A, Tyunina M, Narkilahti J, Levoska J, Chvostova D, Jastribik L, Trepakov VA (2010) Tensile strain induced changes in the optical spectra of $SrTiO_3$ epitaxial thin films. Phys Solid State 52:2082–2089
[54] Erdman N, Poeppelmeier KR, Asta M, Warschkow O, Ellis DE, Marks LD (2002) The structure and chemistry of the TiO_2 rich surface of $SrTiO_3$ (001). Nature 419:55–58
[55] Eglitis RI, Popov AI (2018) Systematic trends in (001) surface ab initio calculations of ABO_3 perovskites. J Saudi Chem Soc 22:459–468
[56] Eglitis RI (2014) Ab initio calculations of $SrTiO_3$, $BaTiO_3$, $PbTiO_3$, $CaTiO_3$, $SrZrO_3$, $PbZrO_3$ and $BaZrO_3$ (001), (011) and (111) surfaces as well as *F* centers, polarons, KTN solid solutions and Nb impurities therein. Int J Mod Phys 28:1430009

[57] Zhang JM, Cui J, Xu KW, Ji V, Man ZY (2007) Ab initio modelling of $CaTiO_3$ (110) polar surfaces. Phys Rev B 76:115426

[58] Heifets E, Kotomin EA, Maier J (2000) Semiempirical simulations of surface relaxation for perovskite titanates. Surf Sci 462:19–35

[59] Bottin F, Finocchi F, Noguera C (2003) Stability and electronic structure of the (1 × 1) $SrTiO_3$ (110) polar surfaces by first-principles calculations. Phys Rev B 68:035418

[60] Heifets E, Goddard WA, Kotomin EA, Eglitis RI, Borstel G (2004) Ab initio calculations of the $SrTiO_3$ (110) polar surface. Phys Rev B 69:035408

[61] Enterkin JA, Subramanian AK, Russell BC, Castell MR, Poeppelmeier KR, Marks LD (2010) A homologous series of structures on the surface of $SrTiO_3$ (110). Nat Mater 9:245–248

[62] Zhang GX, Xie Y, Yu HT, Fu HG (2009) First-principles calculations of the stability and electronic properties of the $PbTiO_3$ (110) polar surface. J Comput Chem 30:1785–1798

[63] Zhang JM, Pang Q, Xu KW, Ji V (2009) First-principles study of the (110) polar surface of cubic $PbTiO_3$. Comput Mater Sci 44:1360–1365

[64] Xie Y, Yu HT, Zhang GH, Fu HG, Sun JZ (2007) First-principles investigation of stability and structural properties of the $BaTiO_3$ (110) polar surface. J Phys Chem C 111:6343–6349

[65] Wang J, Tang G, Wu XS (2012) Thermodynamic stability of $BaTiO_3$ (110) surfaces. Phys Status Solidi B 249:796–800

[66] Eglitis RI, Rohlfing M (2010) First-principles calculations of the atomic and electronic structure of $SrZrO_3$ and $PbZrO_3$ (001) and (011) surfaces. J Phys Condens Matter 22:415901

[67] Chen H, Xie Y, Zhang GH, Yu HT (2014) A first-principles investigation of the stability and electronic properties of SrZrO3 (110) (1 × 1) polar terminations. J Phys Condens Matter 26:395002

[68] Eglitis RI (2007) First principles calculations of $BaZrO_3$ (001) and (011) surfaces. J Phys Condens Matter 19:356004

[69] Heifets E, Ho J, Merinov B (2007) Density functional simulation of the $BaZrO_3$ (011) surface structure. Phys Rev B 75:155431

[70] Crosby LA, Kennedy RM, Chen BR, Wen JG, Poeppelmeier KR, Bedzyk JM, Marks LD (2016) Complex surface structure of (110) terminated strontium titanate nanododecahedra. Nanoscale 8:16606–16611

[71] Lee C, Yang W, Parr RG (1988) Development of the Colle–Salvetti correlation-energy formula into a functional of the electron density. Phys Rev B 37:785–789

[72] Saunders VR, Dovesi R, Roetti C, Causa N, Harrison NM, Orlando R, Zicovich-Wilson CM (2014) CRYSTAL-2009 user manual. University of Torino, Torino, Italy

[73] Becke AD (1993) Density-functional thermochemistry. III. The role of exact exchange. J Chem Phys 98:5648–5652

[74] Monkhorst HJ, Pack JD (1976) Special points for Brillouin-zone integrations. Phys Rev B 13:5188–5192

[75] Eglitis RI (2015) Theoretical modelling of the energy surface (001) and topology of $CaZrO_3$ perovskite. Ferroelectrics 483:75–85

[76] Tasker PW (1979) The stability of ionic crystal surfaces. J Phys C 12:4977–4984

[77] Pojani A, Finocchi F, Noguerra C (1999) Polarity of the $SrTiO_3$ (111) and (110) surfaces. Surf Sci 442:179–198

[78] Catlow CRA, Stoneham AM (1983) Ionicity in solids. J Phys C Solid State Phys 16:4321–4338

[79] Bochicchio RC, Reale HF (1993) On the nature of crystalline bonding: extension of statistical population analysis to two- and three-dimensional crystalline systems. J Phys B At Mol Opt Phys 26:4871–4883

Institute of Solid State Physics, University of Latvia as the Center of Excellence has received funding from the European Union's Horizon 2020 Framework Programme H2020-WIDESPREAD-01-2016-2017-TeamingPhase2 under grant agreement No. 739508, project CAMART²